Acta Crystallographica Section F
Structural Biology and Crystallization Communications
ISSN 1744-3091

Crystallization and diffraction analysis of *β*-*N*-acetylhexosaminidase from *Aspergillus oryzae*

Ondřej Vaněk,[a,b] Jiří Brynda,[c,d] Kateřina Hofbauerová,[a] Zdeněk Kukačka,[a,b] Petr Pachl,[d] Karel Bezouška[a,b] and Pavlína Řezáčová[c,d]*

[a]Institute of Microbiology, Academy of Sciences of the Czech Republic, Vídeňská 1083, 14220 Prague, Czech Republic, [b]Department of Biochemistry, Faculty of Science, Charles University in Prague, Hlavova 8, 12840 Prague, Czech Republic, [c]Institute of Organic Chemistry and Biochemistry, Academy of Sciences of the Czech Republic, Flemingovo nám. 2, 16610 Prague, Czech Republic, and [d]Institute of Molecular Genetics, Academy of Sciences of the Czech Republic, Vídeňská 1083, 14220 Prague, Czech Republic

Correspondence e-mail: rezacova@img.cas.cz

Received 27 December 2010
Accepted 9 February 2011

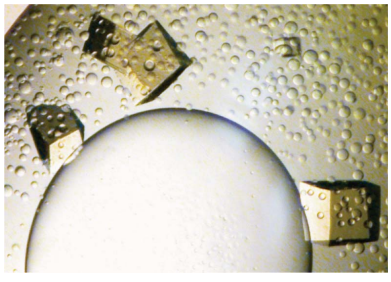

© 2011 International Union of Crystallography
All rights reserved

Fungal *β*-*N*-acetylhexosaminidases are enzymes that are used in the chemoenzymatic synthesis of biologically interesting oligosaccharides. The enzyme from *Aspergillus oryzae* was produced and purified from its natural source and crystallized using the hanging-drop vapour-diffusion method. Diffraction data from two crystal forms (primitive monoclinic and primitive tetragonal) were collected to resolutions of 3.2 and 2.4 Å, respectively. Electrophoretic and quantitative N-terminal protein-sequencing analyses confirmed that the crystals are formed by a complete biologically active enzyme consisting of a glycosylated catalytic unit and a noncovalently attached propeptide.

1. Introduction

Fungal *β*-*N*-acetylhexosaminidases (EC 3.2.1.52) are robust extracellularly secreted enzymes which play a crucial physiological role in the complex chitinolytic system in the cell wall of the growing fungus (Slámová *et al.*, 2010). They cleave chitobiose into the constituent monosaccharides (Huňková *et al.*, 1996). These enzymes are physiologically crucial during the life cycle of the fungus for the formation of septa, germ tubes and fruit bodies (Gooday *et al.*, 1992; Bulawa, 1993; Cheng *et al.*, 2000). These processes are important in the control of fungal and insect pests (Cohen, 2001) and are also relevant to human diseases (Mahuran, 1999), leading to considerable interest in the catalytic mechanism of these enzymes. The fungal enzymes are mostly utilized in chemoenzymatic synthesis of biologically interesting oligosaccharides using their effective transglycosylation of *β*-GlcNAc and *β*-GalNAc (Křen *et al.*, 1994; Rajnochová *et al.*, 1997; Krist *et al.*, 2001; Weignerová *et al.*, 2003).

The production of the natural enzyme from *Aspergillus oryzae* is highly induced by the presence of GlcNAc in the cultivation medium (Huňková *et al.*, 1996). Biochemical studies of this enzyme revealed an interesting and complex protein architecture in which the N-glycosylated catalytic unit associates with the O-glycosylated propeptide to produce the functional enzyme that is secreted into the extracellular environment (Plíhal *et al.*, 2007). The large propeptide of this enzyme (containing 78 amino-acid residues) has been characterized as a novel class of enzyme regulator that must be processed intracellularly in order to control activity, dimerization and secretion (Plíhal *et al.*, 2007).

Fungal hexosaminidases from closely related species such as *Penicillium oxalicum* appear to share both high sequence similarity and other structural features such as the arrangement of disulfides with the *A. oryzae* enzyme, which is the most extensively studied (Pompach *et al.*, 2009). The sequence similarity of the *A. oryzae* *β*-*N*-acetylhexosaminidase to enzymes from other fungal species is about 85%; its sequence similarity to bacterial and human enzymes ranges from 42 to 49% (Plíhal *et al.*, 2007).

The three-dimensional structure of fungal hexosaminidases has to date only been characterized by computer modelling, vibrational spectroscopy and biochemical approaches (Ettrich *et al.*, 2007). The catalytic domain of *β*-*N*-acetylhexosaminidase (499 amino-acid residues forming an *α*/*β* TIM barrel) is highly conserved in hexosaminidases from all sources examined to date, allowing the construction of a plausible molecular model for the *A. oryzae* enzyme

(Ettrich *et al.*, 2007). However, neither molecular-modelling techniques nor the solved crystal structures of homologous enzymes from the bacteria *Serratia marcescens* (PDB entry 1c7s; Prag *et al.*, 2000) and *Streptomyces plicatus* (PDB entry 1jak; Mark *et al.*, 2001) and from human (PDB entry 1now; Mark *et al.*, 2003) could provide any information on the spatial position of the propeptide.

Along these lines of research, we have now initiated experiments towards the crystallization of the enzyme and the determination of the structure of *β*-*N*-acetylhexosaminidase from *A. oryzae* by X-ray crystallography. Here, we report our initial results describing crystallization and diffraction data analysis.

2. Materials and methods

2.1. Protein expression and purification

The molecular cloning and sequencing of the *β*-*N*-acetylhexosaminidase gene (GenBank accession No. AY091636) has been described previously (Plíhal *et al.*, 2007). *A. oryzae* strain CCF 1066 (Czech Collection of Fungi, Department of Botany, Charles University, Prague) was grown in a minimal medium consisting of 0.3%(*w*/*v*) KH_2PO_4, 0.5%(*w*/*v*) $NH_4H_2PO_4$, 0.2%(*w*/*v*) $(NH_4)_2SO_4$, 1.5%(*w*/*v*) NaCl, 0.05%(*w*/*v*) $MgSO_4$, 0.05%(*w*/*v*) yeast extract and 0.5%(*w*/*v*) *N*-acetyl-D-glucosamine at pH 6.0. The fungus was cultivated at 301 K and the medium used for isolation of the secreted native enzyme was collected after 10 d. The crude enzyme obtained by precipitation of the culture medium with ammonium sulfate (80% saturation) was dissolved in 0.6 *M* ammonium sulfate, 20 m*M* sodium phosphate pH 6.8. The enzyme solution was applied onto a Phenyl-Sepharose HP column (2.6 × 10 cm, Amersham Biosciences) equilibrated in the same buffer. The enzyme was eluted with a linear gradient of decreasing ammonium sulfate content (60 min at a 3 ml min^{-1} flow rate). The enzyme was further purified on an SP-Sepharose HR column (1.6 × 5 cm, Amersham Biosciences) equilibrated in 20 m*M* sodium citrate pH 3.5 and eluted with a linear gradient of sodium chloride (20 min at a 2 ml min^{-1} flow rate). The eluted enzyme was concentrated, transferred to 20 m*M* Bis-Tris pH 7.0 buffer and purified to near-homogeneity on a Mono Q column (0.5 × 5 cm, Amersham Biosciences) using a linear gradient of 0–0.5 *M* NaCl (30 min at a 1 ml min^{-1} flow rate). The final purification was achieved on a Superdex 200 HR column (1 × 30 cm, Amersham Biosciences) equilibrated in 20 m*M* sodium citrate pH 5.0, 0.3 *M* NaCl and 1 m*M* sodium azide. The purified enzyme was concentrated to 60 mg ml^{-1} and stored at 253 K. The enzymatic activity and purity of the prepared protein was monitored using the chromogenic substrate 4-nitrophenyl-2-acetamido-2-deoxyglucopyranoside (Ettrich *et al.*, 2007) and SDS–PAGE throughout the whole purification procedure.

2.2. Protein crystallization

The hanging-drop vapour-diffusion method was used to set up all crystallization experiments at 291 K. Initial screening was performed using 24-well Linbro plates; subsequent optimization of crystallization conditions was performed in NeXtal plates (Qiagen) for ease of crystal manipulation. The reservoir contained 1 ml solution and drops were set up by mixing 1 µl protein solution (20 mg ml^{-1} in buffer consisting of 20 m*M* sodium citrate pH 5.0, 0.3 *M* sodium chloride and 1 m*M* sodium azide) and, unless otherwise noted, 1 µl inhibitor solution (10 m*M* NAG-thiazoline in the same buffer) with 1 µl reservoir solution.

Initial grid screening and subsequent optimization were performed with buffer and precipitant stock solutions that were prepared in-house. Alternatively, selected conditions from the Crystallization Basic and Extension Kits for Proteins (Sigma–Aldrich) were used.

Preliminary needle-shaped crystals grew in 20%(*w*/*v*) PEG 3400, 0.1 *M* sodium cacodylate pH 7.0 and 0.3 *M* NaCl.

The optimal crystal of crystal form I used for data collection was obtained from an immiscible mixture of 20%(*w*/*v*) PEG 3400, 2.0 *M* ammonium sulfate, 0.1 *M* sodium citrate pH 5.0 within two weeks. The reservoir solution was mixed thoroughly prior to drop setup.

The optimal crystal of crystal form II used for data collection was obtained using condition No. 39 from the Basic Kit (Sigma–Aldrich) consisting of 2.0 *M* ammonium sulfate, 2%(*w*/*v*) PEG 400, 0.1 *M* HEPES sodium salt pH 7.5 after eight months.

Table 1
Data-collection statistics.

Values in parentheses are for the highest resolution shell.

	Crystal form I	Crystal form II
No. of crystals	1	1
Beamline	Home source (Nonius FR591)	APS 19-ID
Wavelength (Å)	1.54	0.979
Detector	MAR 345	MAR Mosaic 225
Crystal-to-detector distance (mm)	300	225
Rotation range per image (°)	0.5	0.25
Total rotation range (°)	100	112.5
Exposure time per image (s)	900	1
Resolution range (Å)	4.9–3.2 (3.28–3.2)	30–2.3 (2.38–2.3)
Space group	$P2_1$	$P4_12_12$ or $P4_32_12$
Unit-cell parameters		
a (Å)	109.6	105.55
b (Å)	188.8	105.55
c (Å)	117.3	282.74
α (°)	90.0	90.0
β (°)	95.5	90.0
γ (°)	90.0	90.0
Total No. of measured intensities†	169500	460680
No. of unique reflections	66691 (5120)	72108 (7046)
Multiplicity	2.5 (2.4)	6.4 (6.5)
Average $I/\sigma(I)$	6.8 (1.9)	19.3 (2.7)
Completeness (%)	81.2 (84.8)	100 (100)
R_{merge}‡ (%)	19.7 (52.9)	5.9 (79.6)
$R_{p.i.m.}$§ (%)	14.1 (38.9)	7.0 (42.6)
Overall *B* factor from Wilson plot ($Å^2$)	39.7	39.8

† The criterion for observed reflections was $I/\sigma(I) > 0$. ‡ $R_{merge} = 100 \times \sum_{hkl}\sum_i |I_i(hkl) - \langle I(hkl)\rangle| / \sum_{hkl}\sum_i I_i(hkl)$, where $I_i(hkl)$ is an individual intensity of the *i*th observation of reflection *hkl* and $\langle I(hkl)\rangle$ is the average intensity of reflection *hkl* with summation over all data. § $R_{p.i.m} = 100 \times \sum_{hkl}[1/(N-1)]^{1/2} \times \sum_i |I_i(hkl) - \langle I(hkl)\rangle| / \sum_{hkl}\sum_i I_i(hkl)$, where *N* is the number of times the given reflection *hkl* was observed (Weiss, 2001).

2.3. Protein-crystal analyses

For analyses, the crystals were removed from their mother liquor using a nylon loop, washed in reservoir solution and dissolved in water. The protein content of the crystals was analyzed by SDS–PAGE and quantitative protein sequencing.

For the latter analysis, a solution containing dissolved crystals was applied onto a BioBrene precycled protein filter (Applied Biosystems) and subjected to ten cycles of automated Edman degradation in a Procise 491 protein sequencer (Applied Biosystems). Chromatograms from individual cycles were integrated using the *SequencePro* software supplied by the instrument manufacturer and the yields were related to the PTH amino-acid standard.

2.4. Diffraction data collection

For diffraction data collection, the crystals were flash-cooled in liquid nitrogen. For cryoprotection, the crystals were soaked for 10 s

in the corresponding reservoir solution supplemented with 25%(*v*/*v*) glycerol.

Diffraction data for crystal form I (monoclinic) were collected at 120 K on a MAR345 image-plate system using a Nonius FR591 rotating-anode generator. The diffraction data were integrated and reduced using *MOSFLM* (Leslie, 1999) and scaled using *SCALA* (Evans, 2006) from the *CCP*4 suite (Collaborative Computational Project, Number 4, 1994). The crystal parameters and data-collection statistics are summarized in Table 1.

Diffraction data for crystal form II (tetragonal) were collected at 100 K on beamline 19-ID of the Structural Biology Center at the Advanced Photon Source, Argonne National Laboratory, Argonne, Illinois, USA. The diffraction data were processed using the *HKL*-3000 suite of programs (Minor *et al.*, 2006). The crystal parameters and data-collection statistics are summarized in Table 1.

3. Results and discussion

The *β*-*N*-acetylhexosaminidase secreted by *A. oryzae* into the culture medium (hereafter referred to as HEX) was produced and purified to near-homogeneity according to a published protocol (Plíhal *et al.*, 2007) with minor modifications as described in §2.1. The purity of the final protein preparation was assessed by SDS–PAGE (Fig. 1*a*). The enzyme is composed of a main catalytic subunit (499 amino-acid residues, 56.9 kDa) and a propeptide (78 amino-acid residues, 8.1 kDa) which is noncovalently attached to the main subunit (Plíhal *et al.*, 2007). The expected molecular weight of the native enzyme is higher owing to N-glycosylation; it has been shown that all six potential N-glycosylation sites are occupied by high-mannose-type oligosaccharides, with the hexamannosyl oligosaccharide being the predominant structure (Ettrich *et al.*, 2007). Thus, approximately an 8 kDa increase in the observed protein molecular weight might be expected (Fig. 1*a*). The enzyme forms a stable dimer in solution as shown by gel filtration as well as native electrophoresis (Plihal *et al.*, 2007).

While being highly pure with respect to the absence of macromolecular contaminants, the final concentrated protein sample was of a dark brown colour. This colour was most probably caused by a noncovalent association of some compounds originating either from the cultivation medium or produced by the fungus itself during cultivation. The chemical identity of these compounds is unknown, but their procurement and retention through several chromatographic purification steps indicate that these compounds bind to the HEX protein with high affinity. Despite this, the prepared HEX was fully enzymatically active, as observed by the standard assay (Ettrich *et al.*, 2007) with the chromogenic substrate 4-nitrophenyl-2-acetamido-2-deoxyglucopyranoside (data not shown). This observation led us to conclude that the native conformation of the enzyme was not affected and its active site was not blocked by any of the contaminating compounds; we thus used this protein preparation in the subsequent crystallization experiments.

Instead of extensive screening for crystallization conditions, we first considered the conditions successfully used for homologous and functionally related enzymes. Research using the literature and the PDB database (Berman *et al.*, 2000) revealed that all available structures of *β*-*N*-acetylhexosaminidase enzymes (bacterial and human; reviewed by Slámová *et al.*, 2010) had been determined using crystals grown by the hanging-drop vapour-diffusion method under mildly acidic pH conditions, with ammonium sulfate and PEG being the most common precipitants. Glycerol was also often used in crystallization as well as as a cryoprotectant. Based on this, we designed a partial grid screen composed of 48 conditions containing 2.0–3.0 *M* ammonium sulfate or 20–25%(*w*/*v*) PEG 3400 as precipitants screened against various buffers (at pH 4–8) in the presence or absence of 20%(*v*/*v*) glycerol. The protein concentration was 20 mg ml^{-1} in a buffer consisting of 20 m*M* sodium citrate pH 5.0, 0.3 *M* sodium chloride and 1 m*M* sodium azide and the protein solution was mixed with an equal volume of inhibitor solution prior to drop setup.

While ammonium sulfate alone was not able to precipitate HEX at the tested concentrations, the addition of glycerol led to heavy precipitation. In contrast, conditions containing PEG 3400 yielded several successful crystallization events. Six conditions containing PEG 3400 (of the 18 tested) produced needle-shaped crystals, the largest of which grew from 20%(*w*/*v*) PEG 3400, 0.1 *M* cacodylate pH 7.0 and 0.3 *M* NaCl (Fig. 2*a*).

In order to improve the crystal quality, we tested the effect of glycosylation on the crystal size and shape. We enzymatically deglycosylated HEX by treatment with endoglycosidase H under native conditions (Ettrich *et al.*, 2007) and used the deglycosylated protein in crystallization trials. However, no other crystal form apart from the needle-shaped crystals was observed for the deglycosylated enzyme. Therefore, we continued to work with the natively glycosylated enzyme.

In the next round of optimization, an extensive screening exploring the effect of a range of concentrations of ammonium sulfate and PEG 3400 and of PEG of various molecular weights, the pH and the use of additives and ions was performed. We also tested conditions containing both precipitants (ammonium sulfate and PEG 3400) together in varying ratios. This led to the identification of new crystallization conditions that yielded three-dimensional protein crystals of brown colour. These crystals grew from a reservoir containing an immiscible mixture of 20–25%(*w*/*v*) PEG 3400 or PEG 8000 and 1.0–2.0 *M* ammonium sulfate in the presence of 0.1 *M* sodium cacodylate pH 7.0 and 0.3 *M* NaCl. The reservoir solutions were mixed thoroughly prior to their addition to the hanging drops in order to obtain an even emulsion of both precipitant phases. However, the drops were clear after setup owing to the initial dilution by the protein and inhibitor solutions. During the vapour-diffusion-driven concentration of the

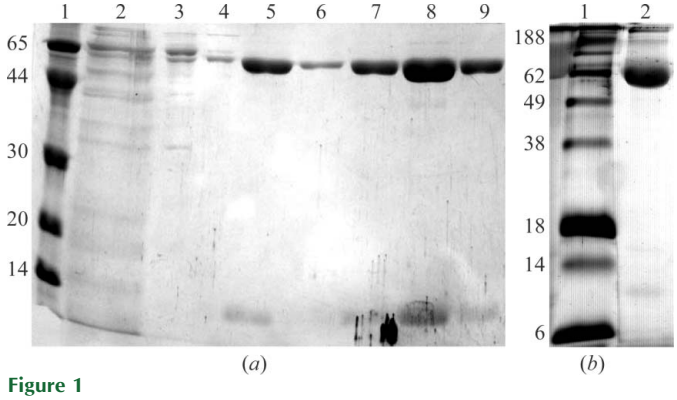

Figure 1
Analysis of HEX protein and crystals by SDS–PAGE. The glycosylated enzyme catalytic subunit and noncovalently associated propeptide migrated at the expected molecular weights of 63 and 8 kDa, respectively. (*a*) 15% SDS–PAGE stained by Coomassie Brilliant Blue R-250 was used to follow the HEX sample composition and purity during the purification procedure. Lane 1, home-made molecular-weight markers (kDa); lane 2, crude extract; lane 3, after phenyl Sepharose purification; lane 4, after SP Sepharose purification; lane 5, after Mono-Q purification; lanes 6–9, fractions from gel filtration on Superdex 200. Fractions from gel filtration were pooled and used for crystallization. (*b*) Silver-stained 15% SDS–PAGE was used to analyze the protein composition of dissolved crystal form II. Lane 1, SeeBlue Pre-Stained Standard molecular-weight markers (Invitrogen) (kDa); lane 2, dissolved crystal.

drops placed above the reservoir, phase separation appeared and crystal nucleation often occurred at the boundary of the two phases. The typical crystal morphology is represented by crystals grown in 20%(*w*/*v*) PEG 3400, 1.4 *M* ammonium sulfate, 0.1 *M* cacodylate pH 7.0 and 0.3 *M* NaCl (Fig. 2*b*) and 20%(*w*/*v*) PEG 3400, 2.0 *M* ammonium sulfate and 0.1 *M* sodium citrate pH 5.0 (Fig. 2*c*). The crystals depicted in Fig. 2(*c*), with dimensions of about 0.25 × 0.25 × 0.1 mm, were used to collect a complete data set to a resolution limit of 3.2 Å at 120 K using an in-house rotating-anode X-ray source (Fig. 3*a*). The crystals exhibited the symmetry of space group $P2_1$. Crystal parameters and data-collection statistics for this crystal form (form I) are summarized in Table 1. Evaluation of the crystal-packing parameters indicated the presence of six or seven molecules in the asymmetric unit, with corresponding solvent contents of 57 or 50% and Matthews coefficients of 2.88 or 2.47 $Å^3\ Da^{-1}$, respectively (Matthews, 1968).

In an attempt to further improve the resolution and to possibly identify different crystallization conditions and HEX crystal forms, 24 selected conditions from the Crystallization Basic and Extension Kits for Proteins (Sigma–Aldrich) were tested, including most of the ammonium and lithium sulfate-based conditions and their combination with PEG solutions. In this case, the protein solution was mixed with the protein buffer instead of the inhibitor solution. While almost all of the drops precipitated heavily upon drop setup, condition No. 39 from the Basic Kit consisting of 2.0 *M* ammonium sulfate, 2%(*w*/*v*) PEG 400, 0.1 *M* HEPES sodium salt pH 7.5 yielded three-dimensional protein crystals of brown colour with a different morphology after eight months (Fig. 2*d*). As the crystals appeared after an extended period of time, we analyzed the protein crystals in order to reveal any protein degradation during the crystallization process. Analysis of the protein content was performed by SDS–PAGE analysis of dissolved crystals. The protein composition of the crystals was very similar to that observed in the protein solution used for crystallization (Fig. 1). The glycosylated enzyme catalytic subunit and noncovalently associated propeptide migrated at the expected molecular weights of 63 and 8 kDa, respectively. Because variable proportions of the propeptide may occur in purified HEX preparations depending on the cultivation conditions of the producing organism, we also determined the ratio between the catalytic subunit and the propeptide (Plíhal *et al.*, 2007). We used quantitative Edman degradation in the protein sequencer, an analysis which is rarely performed but which has proved to be useful for evaluation of the reconstitution efficiency of HEX (Plíhal *et al.*, 2007) as well as for polypeptide quantification (Brune *et al.*, 2007). The results of analysis performed on dissolved crystals revealed an equimolar content of the propeptide and the catalytic unit, clearly indicating full saturation of the catalytic unit by the propeptide (Table 2). These analyses thus proved that the crystals contain complete biologically active enzyme.

Crystals with dimensions of about 0.3 × 0.15 × 0.15 mm were used to collect a complete data set to 2.4 Å resolution at 100 K on

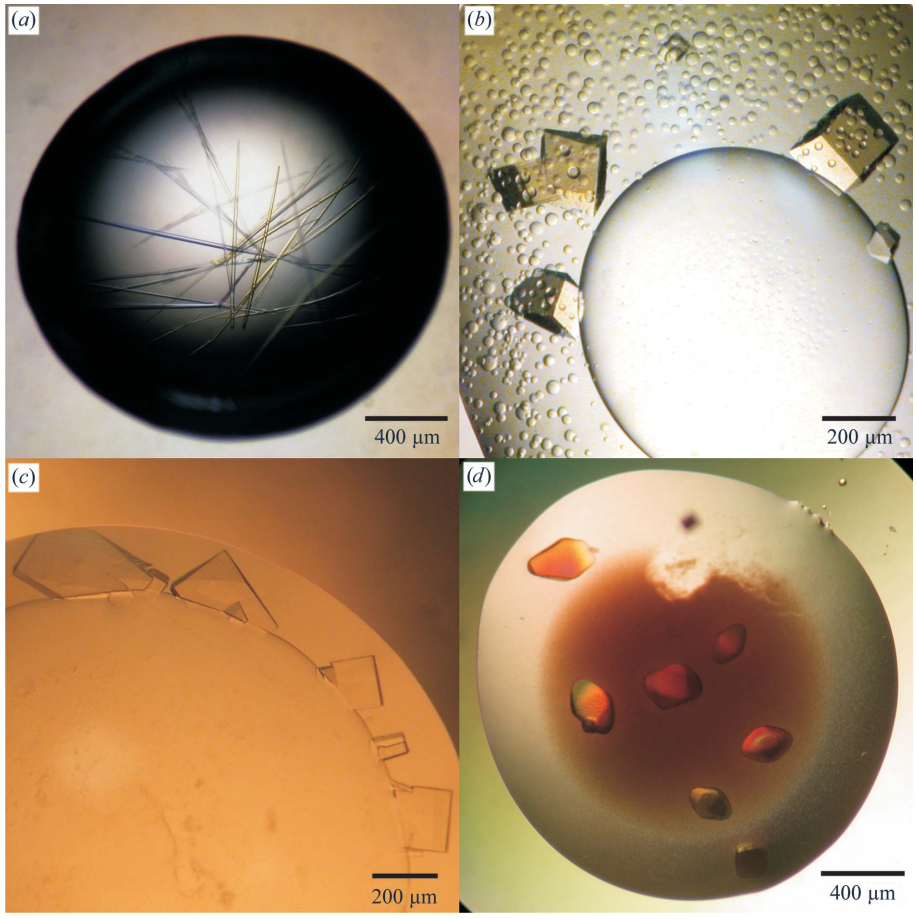

Figure 2
Crystals of HEX. (*a*) Initial crystals obtained from screening for crystallization conditions [20%(*w*/*v*) PEG 3400, 0.1 *M* cacodylate pH 7.0 and 0.3 *M* NaCl]. (*b*) Crystals grown from optimized conditions [20%(*w*/*v*) PEG 3400, 1.4 *M* ammonium sulfate, 0.1 *M* cacodylate pH 7.0 and 0.3 *M* NaCl]. (*c*) Crystals of monoclinic crystal form I grown from optimized conditions [20%(*w*/*v*) PEG 3400, 2.0 *M* ammonium sulfate, 0.1 *M* sodium citrate pH 5.0] and used for data collection. (*d*) Crystals of tetragonal crystal form II grown from optimized conditions [2.0 *M* ammonium sulfate, 2%(*w*/*v*) PEG 400, 0.1 *M* HEPES sodium salt pH 7.5] and used for data collection.

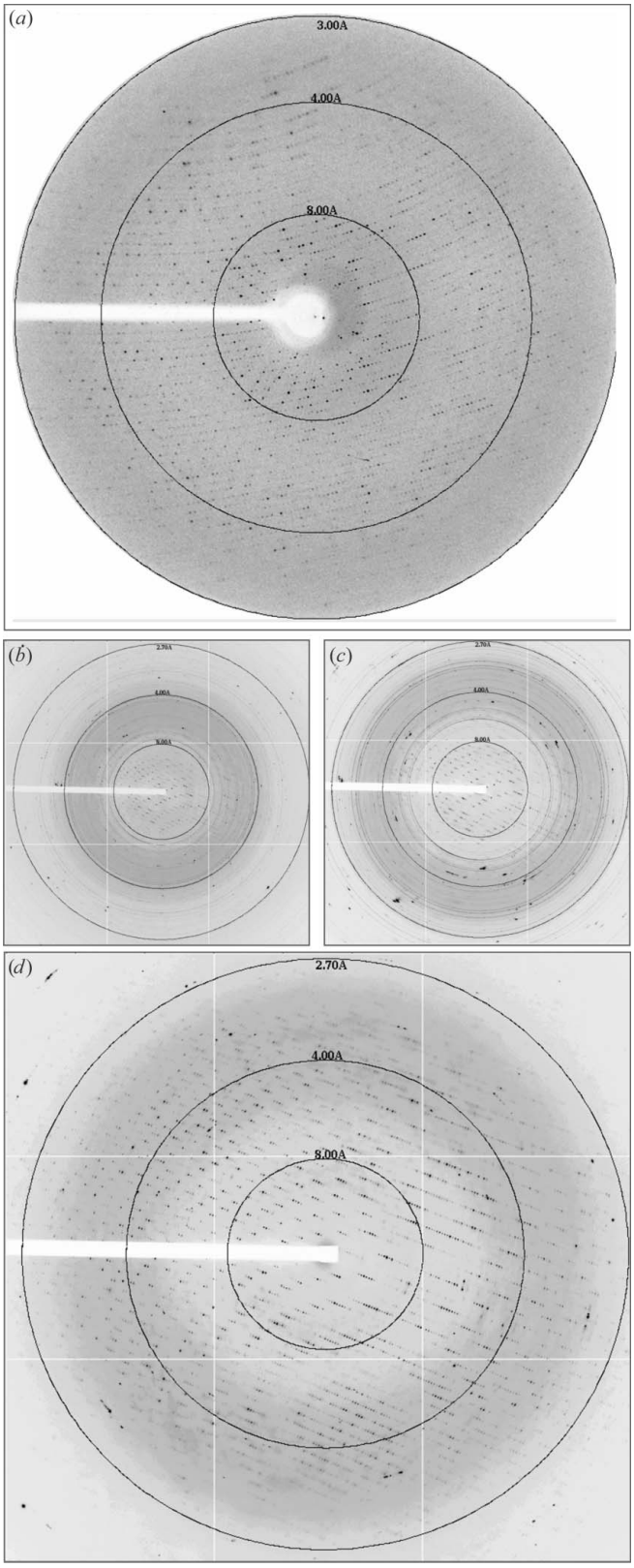

Figure 3
Diffraction images from HEX crystals. (*a*) Diffraction image collected using a home-source rotating-anode generator for the monoclinic crystal form I. (*b*–*d*) Diffraction images collected at a synchrotron source from the tetragonal crystal form II upon repeated crystal annealing: (*b*) diffraction image from crystal upon cryocooling, (*c*) diffraction image after crystal annealing performed by blocking the cryostream for 3 s, (*d*) diffraction image after repeated crystal annealing. After the second annealing, the complete data set was collected.

Table 2
Crystal analysis by N-terminal sequencing.

	Propeptide		Catalytic subunit		
Cycle	Amino acid	C1 (pmol)	Amino acid	C2 (pmol)	Ratio C1/C2
1	Val	69.52	Ala	80.41	0.865
2	Gly	74.25	Ser	37.26†	1.992†
3	Val	64.05	Asn	51.51	1.243
4	Asn	63.74	Ser	29.73†	2.143†
5	Pro	44.96	Leu	46.35	0.970
6	Leu	51.35	Gln	50.64	1.014
7	Pro	41.94	Tyr	48.04	0.873
8	Ala	58.40	Val	48.81	1.196
9	Pro	31.66	Asn	44.65	0.709
10	Arg	39.97	Val	48.59	0.823
Average	—	—	—	—	0.961

† Serine is degraded during Edman sequencing, thus these ratios were not considered in determining the average propeptide to catalytic unit ratio.

beamline 19-ID of the Structural Biology Center at the Advanced Photon Source, Argonne National Laboratory (Argonne, Illinois, USA). A repeated crystal-annealing procedure performed by blocking the cryostream for 3 s was used to improve the diffraction quality. While the diffraction image taken from a cryocooled crystal showed protein diffraction to a resolution of ∼8 Å, after the first and second annealing the diffraction limit was extended to ∼4 and 2.4 Å, respectively (Figs. 3*b*–3*d*). The annealing procedure also significantly improved the diffraction-pattern background. The crystal exhibited the symmetry of point group *P*422, with systematic absences indicating the presence of a 4_1 or 4_3 screw axis. Crystal parameters and data-collection statistics for crystal form II are summarized in Table 1. Evaluation of the crystal-packing parameters indicated the presence of two molecules in the asymmetric unit, with a solvent content of 54% and a Matthews coefficient of 2.67 $Å^3$ Da^{-1} (Matthews, 1968). As a stable dimer was observed for HEX over a wide range of pH (Plíhal *et al.*, 2007), it is likely that the asymmetric unit contains a dimeric biologically active unit.

The diffraction data will be used to determine the HEX structure by molecular replacement using the available structures of homologous enzymes (Slámová *et al.*, 2010). The structure determination will provide important clues to the architecture of fungal *β-N*-acetylhexosaminidases.

This work was supported by projects Z40550506, Z50520514 and AVOZ50200510 awarded by the Academy of Sciences of the Czech Republic and projects MSM21620808 and 1M0505 from the Ministry of Education of the Czech Republic. Use of the Advanced Photon Source was supported by the US Department of Energy, Office of Science, Office of Basic Energy Sciences under Contract No. DE-AC02-06CH11357. The authors wish to thank the members of the Structural Biology Center at Argonne National Laboratory for their help with conducting data collection on the 19-ID beamline, Jiří Janovský for the quantitative Edman degradation experiment and Devon Maloy for critical proofreading of the manuscript.

References

Berman, H. M., Westbrook, J., Feng, Z., Gilliland, G., Bhat, T. N., Weissig, H., Shindyalov, I. N. & Bourne, P. E. (2000). *Nucleic Acids Res.* **28**, 235–242.
Brune, D. C., Hampton, B., Kobayashi, R., Leone, J. W., Linse, K. D., Pohl, J., Thoma, R. S. & Denslow, N. D. (2007). *J. Biomol. Tech.* **18**, 306–320.
Bulawa, C. E. (1993). *Annu. Rev. Microbiol.* **47**, 505–534.
Cheng, Q., Li, H., Merdek, K. & Park, J. T. (2000). *J. Bacteriol.* **182**, 4836–4840.
Cohen, E. (2001). *Pest Manag. Sci.* **57**, 946–950.

Collaborative Computational Project, Number 4 (1994). *Acta Cryst.* D**50**, 760–763.
Ettrich, R., Kopecký, V., Hofbauerová, K., Baumruk, V., Novák, P., Pompach, P., Man, P., Plíhal, O., Kutý, M., Kulik, N., Sklenář, J., Ryšlavá, H., Křen, V. & Bezouška, K. (2007). *BMC Struct. Biol.* **7**, 32.
Evans, P. (2006). *Acta Cryst.* D**62**, 72–82.
Gooday, G. W., Zhu, W.-Y. & O'Donnell, R. W. (1992). *FEMS Microbiol. Lett.* **100**, 387–391.
Huňková, Z., Křen, V., Ščigelová, M., Weignerova, L., Scheel, O. & Thiem, J. (1996). *Biotechnol. Lett.* **18**, 725–730.
Křen, V., Ščigelová, M., Přikrylova, V., Havliček, V. & Sedmera, P. (1994). *Biocatalysis*, **10**, 181–193.
Krist, P., Herkommerová-Rajnochová, E., Rauvolfová, J., Semeňuk, T., Vavrusková, P., Pavlíček, J., Bezouška, K., Petrus, L. & Křen, V. (2001). *Biochem. Biophys. Res. Commun.* **287**, 11–20.
Leslie, A. G. W. (1999). *Acta Cryst.* D**55**, 1696–1702.
Mahuran, D. J. (1999). *Biochim. Biophys. Acta*, **1455**, 105–138.
Mark, B. L., Mahuran, D. J., Cherney, M. M., Zhao, D., Knapp, S. & James, M. N. (2003). *J. Mol. Biol.* **327**, 1093–1109.
Mark, B. L., Vocadlo, D. J., Zhao, D., Knapp, S., Withers, S. G. & James, M. N. (2001). *J. Biol. Chem.* **276**, 42131–42137.
Matthews, B. W. (1968). *J. Mol. Biol.* **33**, 491–497.
Minor, W., Cymborowski, M., Otwinowski, Z. & Chruszcz, M. (2006). *Acta Cryst.* D**62**, 859–866.
Plíhal, O., Sklenář, J., Hofbauerová, K., Novák, P., Man, P., Pompach, P., Kavan, D., Ryšlavá, H., Weignerová, L., Charvátová-Pišvejcová, A., Křen, V. & Bezouška, K. (2007). *Biochemistry*, **46**, 2719–2734.
Pompach, P., Man, P., Kavan, D., Hofbauerová, K., Kumar, V., Bezouška, K., Havlíček, V. & Novák, P. (2009). *J. Mass Spectrom.* **44**, 1571–1578.
Prag, G., Papanikolau, Y., Tavlas, G., Vorgias, C. E., Petratos, K. & Oppenheim, A. B. (2000). *J. Mol. Biol.* **300**, 611–617.
Rajnochová, E., Dvořakova, J., Huňková, Z. & Křen, V. (1997). *Biotechnol. Lett.* **19**, 869–872.
Slámová, K., Bojarová, P., Petrásková, L. & Křen, V. (2010). *Biotechnol. Adv.* **28**, 682–693.
Weignerová, L., Vavrušková, P., Pišvejcová, A., Thiem, J. & Křen, V. (2003). *Carbohydr. Res.* **338**, 1003–1008.
Weiss, M. S. (2001). *J. Appl. Cryst.* **34**, 130–135.